Springer

Journal of
Mechanical
Science and
Technology

Journal of Mechanical Science and Technology 22 (2008) 1359~1373

www.springerlink.com/content/1738-494x

Identification of impact force in thick plates based on the elastodynamics and time-frequency method (II)

- Experimental approach for identification of the impact force based on time frequency methods-

Sung-Jong Kim and Sang-Kwon Lee*

Department of Mechanical Engineering, Inha University, Inchon, 402-751, Korea

(Manuscript Received January 14, 2008; Revised March 19, 2008; Accepted March 21, 2008)

Abstract

The paper presents a novel experimental method for the determination of the impact load in the thick plate based on the theoretical Green's function and the measured waveforms by the sensors arrayed on the surface on the plate. This method requires the location of the impact load. For the accurate estimation of location of impact source in a plate, the arriving time difference between sensors and the propagation velocity of acoustic waveform are necessary. Their measurements are difficult since the acoustic waveforms are dispersive with multi modes in the plate. The time frequency analysis for the acoustic waveform gives the information about the time difference for multi mode dispersive waveform. For the estimation of location of impact source in a plate, the information on the group velocity of the A0 flexible mode is important. In the paper, various time frequency methods are introduced and their methods are compared with simulated signals. The combined higher order time frequency (CHOTF) is employed for dispersive information for the A0 mode flexible mode. The location of impact source and the magnitude of impact load are well estimated based on the theoretical Green's function and the CHOTF for the acoustic waveforms measured by three sensors arrayed on the plate.

Keywords: Green function; Flexible wave; Force identification; Group velocity plate

1. Introduction

The impact load identification problem in the plate has been investigated extensively [1-5]. Michael and Pao [1] developed a method that determined a dynamic force using wave motion measurement. In this case, the location of the impact load was known. In many impact load problems, however, the location of impact load is generally not known. Therefore, in order to identify the location of the impact load, various methods are investigated. In the acoustic emission technique, the standard method of planar source location is to place three or more transducers on the surface of an elastic plate and triangulate the source position by using the differences in arriving times of the acoustic wave at sensors [6-8]. The arriving times are related to the propagation velocity of the acoustic wave. This propagation velocity is therefore important in the estimation of source location. If not taken into account in the measurement of velocity of acoustic wave, highly dispersive propagation can lead to large errors in source location [6]. In the source location problem of impact load, the accurate estimation of propagation velocity of the A_0 flexural mode in plate is difficult since its energy among Lamb modes is dominant [9, 10]. Various techniques for the measurement of velocities of flexural modes have been published in the many research papers [6, 11-15]. Prosser surveys the disadvantages of these techniques well [11]. Recently, after the time-scale method and time-frequency method were employed for the analy-

*Corresponding author. Tel.: +82 32 860 7305, Fax.: +82 32 868 1716
E-mail address: sangkwon@inha.ac.kr
DOI 10.1007/s12206-008-0313-0

sis of the Lamb modes, the group velocity of flexural modes was measured with ease and accuracy in comparison with other convention techniques. Wavelet transform [16], which is representative of the time-scale method, is used in the measurement of the group velocity of flexural mode in a beam [7]. This group velocity is used in detection of the location of impact load. This technique is extended to the detection of the location of impact load in a plate [8]. However, it is known that wavelet transform has bad time-frequency resolution because of the uncertainty principle. In wavelet transform, it is difficult to estimate the group velocity at a narrow frequency band because the frequency step increases with logarithmic scale [17-19]. In this case, the bilinear time-frequency method is the proper method for estimating the group velocity [11, 20, 21]. Prosser employed the pseudo Wigner-Ville distribution (PWVD) method to measure the group velocities of the Lamb modes in the plate [11]. Dispersion measurement from the PWVD can offer a number of advantages in comparison to more traditional measurement techniques. PWVD is, however, sensitive to the background noise because the PWVD uses the second order statistic of acoustic wave data measured in the sensor. Combined higher order time-frequency (CHOTF) method [23, 24] has a strong advantage in detecting the signal with lower signal to noise ratio. In this study, CHOTF is employed to determine the group velocity of flexural mode and to calculate the arriving times of dispersive waves at the sensors installed on the elastic plate to detect the location of impact load. After detecting the location of impact load, theoretical solution to impact load has been used for the determination of impact energy. Gaul and Hurlebaus adapt the classic plate theory (CPT) as a theoretical solution to an impact load after identification of the location of impact load using wavelet transforms [2]. In the determination of the impact energy, there are different approach methods [3, 4]. These methods are based on a structure model to predict the response to impact load. These models characterize the relation between the input and the sensor output. The response comparator compares the measured sensor signal with the predicted model. Sensors are arrayed on the plate. One method uses the strain gauges as sensors [3]. The other uses the piezoelectric film as sensors [4]. These methods use the classic plate theory as a predictive model for predicting the response to an impact load in the structure model. If the thickness of the elastic plate is small,

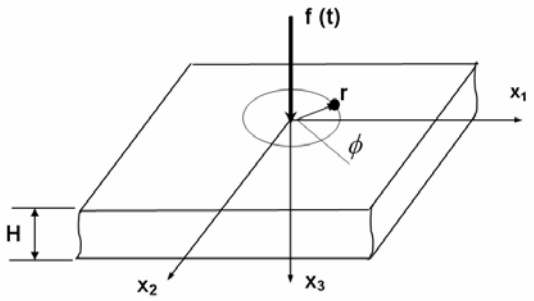

Fig. 1. Geometry of the concentrated load problem.

a sufficiently accurate response can often be obtained through class plastic theory. However, a full elasto-dynamic theory (it is called the exact solution) needs to be employed in the solution of the problem in order to obtain meaningful results or the approximate SDPT, where the transverse shear and rotary inertia are retained in modeling the dynamic deformations cross the thickness of plate [25, 26]. In general, because of being computationally intensive, the approximate SDPT, instead of the exact solution, can be used [27]. In this study, when an impact load excites the plate origin, throughout the measurement of the an acoustic wave at the arbitrary response point of the plate as shown in Fig. 1 and the theoretical Green's function between the impact position and the response, the ability to determine the location and the time history of impact load is demonstrated.

2. Comparison of time frequency methods

In the field of signal processing, Fourier transform (FT) is one of the most useful tools for the spectrum analysis of a wave signal obtained from a structure. However, the FT has been used for stationary signals. The wave propagation of the solid is usually non-stationary signals since the speed of a solid wave depends on the frequency. For the analysis of non-stationary signals, the short time Fourier transform was developed by Koeng in 1948 [28]. The STFT cannot have good time and frequency resolution simultaneously because of the principle of uncertainty [29]. Wigner-Ville distribution [30] is a good solution to get better time and frequency resolution. In this distribution, unwanted cross-terms are generated. It is not a physical term. In order to control the time and frequency resolution depending on frequency and to avoid the occurrence of cross terms, the wavelet transform is employed. The time and frequency reso-

lution is controlled in the wavelet transform [16] with some rule. At low frequency, the time resolution is good and at high frequency, the frequency resolution becomes good. The wave transform is, however, affected by the principle of uncertainty. Therefore, these time-frequency methods each have their advantages and disadvantages. In order to enhance the signal embedded in the background noise, the higher order time frequency method [23] was developed and its origin is based on Wigner distribution. In this session, STFT, Wigner-Ville distribution, wavelet transforms and the higher order time frequency methods are discussed and their characteristics are explained with simulated waveforms and the dispersive wave measured on a simple beam.

2.1 Short time fourier transform

The STFT for signal $s(t)$ is defined by,

$$S(t,f) = \int_{-\infty}^{\infty} h^*(\tau - t)s(\tau)e^{-j2\pi f\tau}d\tau \tag{1}$$

where $h(t)$ is window function. Depending on the size of this moving window, the STFT $S(t, f)$ has different time and frequency resolution. However, if the size of the moving window is fixed, the time and frequency resolution is not controlled in the time-frequency domain. It should satisfy the uncertainty principle [30].

2.2 Wavelet transform

Wavelet transform has been recently used in many fields of engineering work because of its diverse expression. The continuous wavelet transform is defined by

$$\begin{aligned} CWT(\eta,b) &= \int_{-\infty}^{\infty} s(t)\psi^*\left(\frac{t-b}{\eta}\right)dt \\ &= \int s(t)e^{-\left(\frac{t-b}{\eta}\right)^2/\sigma^2} e^{j2\pi\frac{f_0}{\eta}(t-b)}dt \end{aligned} \tag{2}$$

The function $\Psi(t)$ is the mother wavelet given by

$$\psi(t) = Ae^{-\left(\frac{t-b}{\eta}\right)^2/\sigma^2} e^{j2\pi\frac{f_0}{\eta}(t-b)} \tag{3}$$

This mother wavelet is scaled by η in the frequency domain and shifted by b in the time domain. The window size of the wavelet transform is controlled by scaling factor η. f_0 is the fundamental frequency of the mother wavelet and σ is arbitrary constant. f_0 controls the frequency range for the analysis of data. The constant σ controls the window size with η. Since the window size is controlled by constant σ and η, frequency resolution and time resolution are changed depending on frequency. It should, however, satisfy the uncertainty principle.

2.3 Wigner-ville distribution

The bilinear distributions, commonly referred to as Cohen's class, can all be derived from a single distribution, the Wigner-Ville distribution (WVD). The WVD can be defined in two, equivalent fashions:

$$\begin{aligned} W(t,f) &= \int s(t-\tau/2)s^*(t+\tau/2)e^{-2\pi if\tau}d\tau \\ &= \int S(f-\nu/2)S^*(f+\nu/2)e^{-2\pi if\nu}d\nu \end{aligned} \tag{4}$$

where $s(t)$ is the signal being analyzed, $S(f)$ is its Fourier transform and * denotes complex conjugation. The WVD has many desirable properties including the fact that it can yield good time frequency resolution. However, its direct application is limited by the fact that it generates cross-terms. Specifically, the WVD of a signal $s_1(t) + s_2(t)$ contains components due solely to $s_1(t)$ and $s_2(t)$, referred to as the auto-terms, along with an additional interference (cross-) term arising because of the interaction of $s_1(t)$ and $s_2(t)$. They are distinguished from the auto-terms (the components of the distribution which directly relate to input components) by virtue of the fact that the cross-terms are oscillatory, whereas the auto-terms are not. Hence, applying a two dimensional low pass filter to the WVD reduces cross-terms, relative to the auto-terms. The general form of a bilinear time-frequency representation is

$$C(t,f) = \iint W(t,f)\Phi(f,t)dt\,df \tag{5}$$

where $C(t, f)$ is a general bilinear distribution and $\Phi(t, f)$ is a two-dimensional low pass filter. Different choices for the function $\Phi(t, f)$ result in the plethora of bilinear distributions available.

2.4 Higher order time frequency method

The bilinear methods above decompose a signal's energy, *i.e.,* $\int s(t)^2 dt$, into a function of time and frequency. One extension to such analysis techniques is to consider signal decompositions that relate to

higher moments. One decomposes a signal's higher moment, *i.e.,* $\int s(t)^k dt$, where k is some integer greater than two. The auto-terms appear in "unexpected" locations in the time-frequency plane. For this reason, it is common to restrict one's attention to even-order distributions. This paper will concentrate on fourth-order distributions, being next even order greater than two. The WVD can be extended to the Wigner fourth order moment spectra (WFOMS), [31]:

$$W_f(t,f_1,f_2,f_3)=\iiint s^*(t-\tau)s(t-\tau+\tau_1)s^*(t-\tau+\tau_2)s(t-\tau+\tau_3)e^{-2\pi i(f_1\tau_1+f_2\tau_2+f_3\tau_3)}d\tau_1 d\tau_2 d\tau_3 \quad (6)$$

where $\tau = (\tau_1+\tau_2+\tau_3)/4$. Note that this distribution is a function of one time variable and three frequency variables and as such is referred to as a multi-frequency representation. The dual form of this distribution is the multi-time distribution [32]

$$W_t(t_1,t_2,t_3,f)=\iiint S^*(f-\nu)S(f-\nu+\nu_1)S^*(f-\nu+\nu_2)S(f-\nu+\nu_3)e^{-2\pi i(t_1\nu_1+t_2\nu_2+t_3\nu_3)}d\nu_1 d\nu_2 d\nu_3 \quad (7)$$

where $\nu = (\nu_1+\nu_2+\nu_3)/4$. Unlike Eq. (4), Eq. (6) and Eq. (7) define two different distributions, with the roles of time and frequency reversed. Recall that the WVD has complete symmetry in the roles of time and frequency (see Eq. (4)). In Eq. (6) and (7) there is no such symmetry. Each of these distributions is a function of four independent variables. The higher order character of these distributions means that the number of cross-terms generated increases dramatically. To mitigate this, and to ease the problems associated with visualization of functions of four variables, it is common to consider subsets (slices) of these functions. For the multi-frequency distribution one selects the slice $f = f_1 = -f_2 = f_3$ and for the multi-time distribution one sets $t = t_1 = -t_2 = t_3$. Within these subsets, the number of cross-terms generated falls dramatically. However, a new problem is encountered. When using the WVD the cross-terms have an oscillatory nature; this means that a smoothing filter can be used to attenuate them. It can be shown that, under certain circumstances, the (sliced) higher order distributions generate cross-terms, which do not oscillate. These cross-terms are potentially problematic since they cannot be attenuated by the use of smoothing. Such cross-terms require an alternative approach to their reduction. The sliced forms of the multi-frequency and multi-time distributions can be respectively expressed as

$$SW_f(t,f)=\int S(f-\nu/4)^2 S^*(f+\nu/4)^2 e^{-2\pi i\nu t}d\nu \quad (8)$$

$$SW_t(t,f)=\int s(t-\tau/4)^2 s^*(t+\tau/4)^2 e^{-2\pi if\tau}d\tau \quad (9)$$

These forms of the representations have been chosen since they most clearly illustrate the connections with the WVD [31, 32]. The above signal representations can be thought of as decompositions of a signal fourth moment, since

$$\iint SW_t(t,f)dtdf=\int |s(t)|^4 dt \quad \text{and}$$

$$\iint SW_f(t,f)dtdf=\int |S(f)|^4 df \quad (10)$$

For the fourth moment there is no equivalent of Parseval's theorem, *i.e.,*

$$\int |S(f)|^4 df \neq \int |s(t)|^4 dt \quad (11)$$

This highlights that Eq. (8) and Eq. (9) are different representations; they are decompositions of different quantities. From Eq. (6) and Eq. (7), one can obtain an intuitive indication of which classes of signals the methods are most suited for. Consider the $SW_f(t, f)$ of a narrow band signal, so that its contribution is centered on some peak in the Fourier transform, then the operation of squaring the Fourier transform, seen in Eq. (8), will serve to accentuate this peak. Similarly, the operations involved in the $SW_t(t, f)$ serve to accentuate short duration transient signals. The former distribution is referred to as the sliced Wigner fourth order moment spectra (SWFOMS) [23]. The latter distribution was initially proposed as one of a more general class of distributions referred to as the L-Wigner distributions (LWD) [33]; to reflect this the $SW_t(t, f)$ will be referred to as the L-Wigner distribution (LWD). An alternative approach to cross-term reduction is required for the higher order distributions. One method proposed for achieving this is based on the observation that

$$SW_f(t,f)=\frac{1}{2}\int W(f,t-\tau)W(f,t+\tau)d\tau \quad (12a)$$

$$SW_t(t,f)=\frac{1}{2}\int W(t,f-\nu)W(t,f+\nu)d\nu \quad (12b)$$

That is, the SWFOMS can be obtained by convolving, with respect to time, the second order WVD whilst the LWD can be obtained by convolving, with respect to frequency. A natural extension to Eq. (12) is to say that generalized versions of the SWFOMS

and the LWD are given by

$$SSW_f(t,f) = \frac{1}{2}\int h(\tau)^2 C(f,t-\tau)C(f,t+\tau)d\tau \quad (13a)$$

$$SSW_t(t,f) = \frac{1}{2}\int H(\nu)^2 C(t,f-\nu)C(t,f+\nu)d\nu \quad (13b)$$

where $C(t, f)$ is any bilinear distribution as described by Eq. (5), and $h(t)$ and $H(f)$ are windowing functions, respectively. If the bilinear distribution has been suitably smoothed, so that its cross-terms have been removed, then prudent choice of the weighting function ensures that no additional cross-terms are generated and that the SWFOMS and LWD are essentially cross-term free [34, 35]. In reference [34, 35] one is advised to select $h(t)$ and $H(f)$ as a rectangular window, the width (in time and frequency) should be no more than the minimum separation between two components. Evidently, the cross-term reduction is highly effective even for the non-oscillating components. According to previous work [36], the SWOFM is not affected by non-oscillated cross-terms along the frequency axis but along the time axis. The LWD is not affected by non-oscillated cross-terms along the time axis. Therefore, when the frequency separation is important, SWOFM is a good solution to represent a non-stationary signal, and when the time separation is important, the LWD is a good selection to present a non-stationary signal. For dispersive Lamb mode waves, at very low frequency, SWOFM is better than LWD, but at high frequency LWD is better than SWOFM. For representation for A_0 mode flexible mode, at first step, SWOFM is employed and at next step LWD is used. Therefore, the high order time frequency presentation of these two-steps defines the combined higher order time-frequency (CHOTF) [22]. At the first step, the selection of time window $h(t)$ is

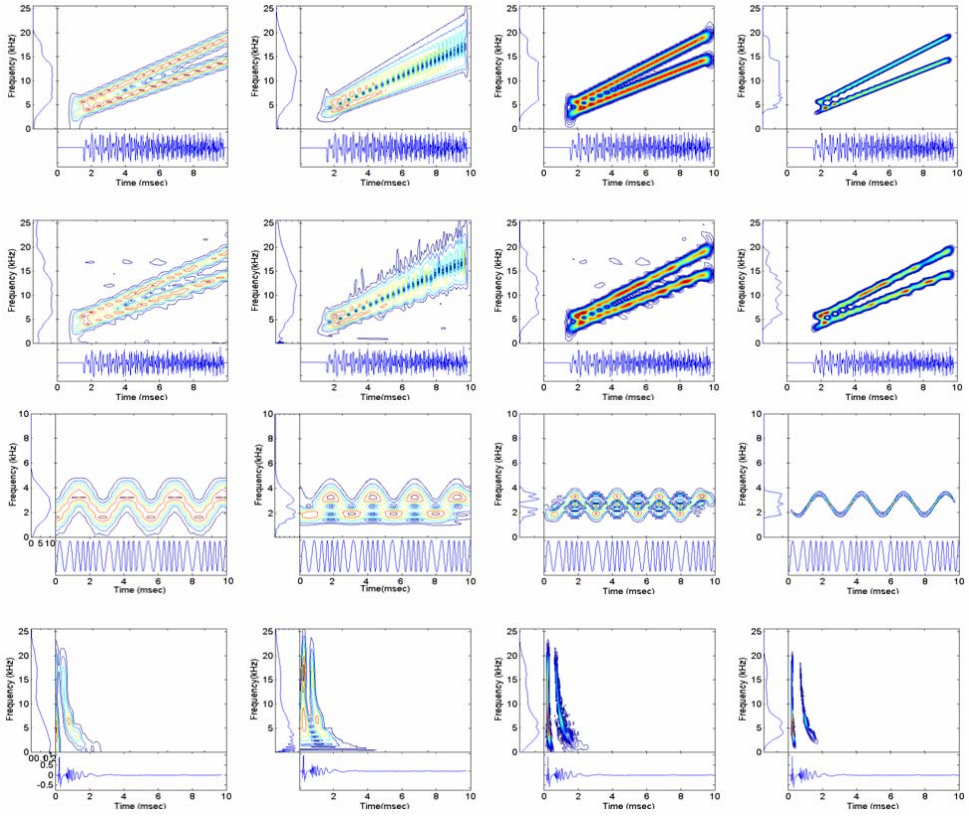

(a) (b) (c) (d)

Fig. 2. Comparison of the time-frequency methods for the simulated signals: figures of the first row are the image analysis for two chirp signals without noise; figures of the second row are the image analysis for two chirp signals data with noise; figures of the third row are the image analysis for frequency modulated signal; figures of the bottom row are the image analysis for the dispersive signal measured in the beam, (a) STTF (b) WT(c) PWD (d) CHOTF.

important and at the next step, the selection of frequency $H(f)$ is important.

3. Numerical results

Fig. 2 explains the characteristics of various time-frequency methods with image analysis in time-frequency domain for three simulated signals and one measured. The figures in the first row are the image analysis for the two simulated chirp signals without background noise. The figures in the second row are the image analysis for the two simulated chirp signals with noise. The figures in the third row are the image analysis for the simulated frequency-modulation signal, which is $x=exp\ (j2\pi f)$ and $f = b\ cos\ (at)+ct$, where a =0.05, b=0.4, c =0.05. The figures in the bottom row are the image analysis for a dispersive wave measured on the beam. Fig. 2(a), (b), (c) and (d) show the STFT, WT, PWD, and CHOFT for each signal, respectively. Fig. 2(a) shows that STFT has bad time and frequency presentations since from Fig. 2(b), WT has bad frequency discrimination at high frequency and has bad time discrimination at low frequency. In Fig. 2(c), we find the PWD has good time and frequency presentation. However, it has still less time frequency presentation than CHOFT, as shown in Fig. 2(d). Especially, from the analysis of a dispersive wave, it is found that the CHOFT is the best method for the identification of the wave propagation. Throughout this paper, the CHOFT is used for the image analysis of the propagation wave measured in the plate. Fig. 3 shows image analysis for two simulated Green's functions obtained by using exact theory and approximated SDPT [38]. For these image analyses, the CHOFT is employed for the two simulated signals. The time-frequency presentation for A0 flexible mode is clear. However, the CHOFT for a simulated Green's function using exact solution also shows the time-frequency presentation for the other flexible mode A1. The time-frequency presentation for the symmetric mode S0 and S1 is not clear since the impact is vertical direction as shown in Fig. 1. In this paper, for the estimation of impact load in the plate, the measurement of the group velocity for the A0 flexible mode is required and the group velocity of this mode is associated with the peak line of image analysis in the time-frequency domain.

4. Location of impact load

For the experiment, an aluminum plate was used, with dimensions 1200mm × 1200mm and 10mm. The impact load was excited by the impact hammer with aluminum tip. The details of experiment are discussed in reference [38]. Fig. 4 shows the comparison between the simulated waveform using SDPT and measured waveform. These waveforms are measured at the position S_0 = 447mm, S_1 = 447mm, and S_2 = 200mm from impact position. The waveforms in the top line are non-filtered waves and the waveforms in the bottom are filtered waveforms. The measured waveforms show reflected wave whilst the simulated waveform has only direct waves in infinite plate. The waveforms measured at sensor S_0 and sensor S_1 are

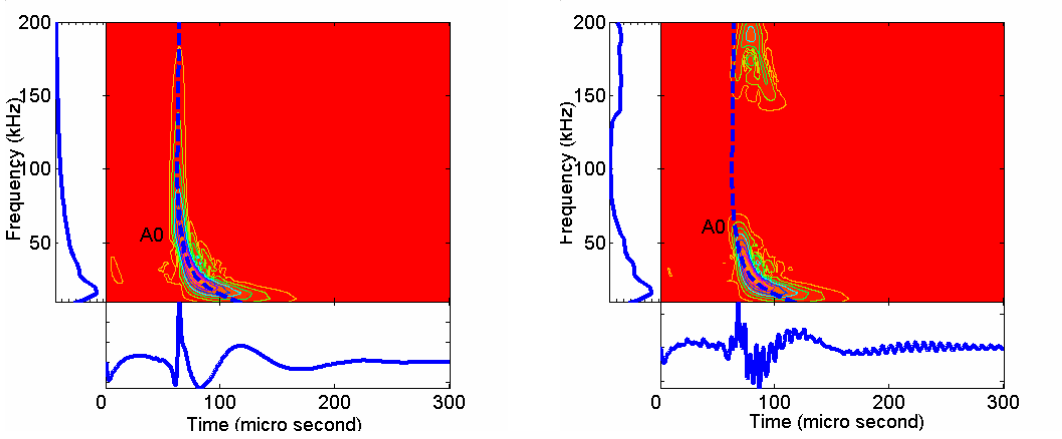

Fig. 3 CHOTF analysis for Green' function (a) Simulated waveform using approximate SDPT (b) Simulated waveform using Exact solution.

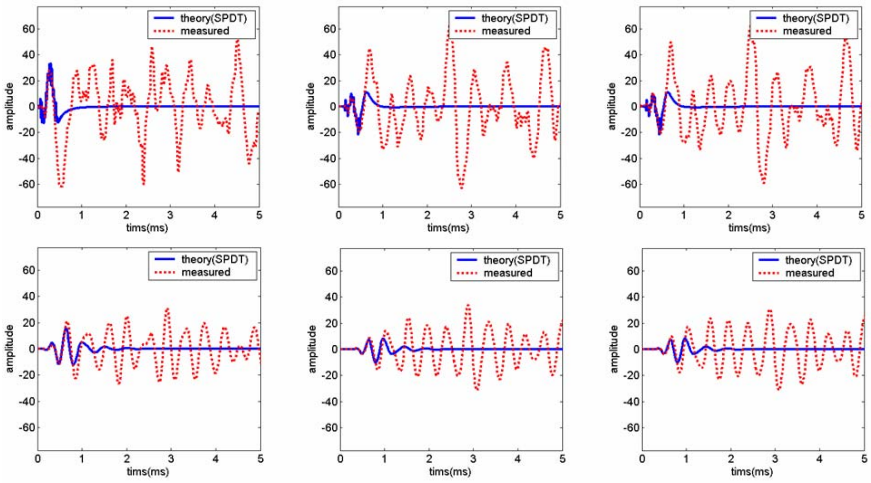

Fig. 4. Comparison between the simulated waveform using SDPT and measured waveform.

affected earlier by reflected wave than waveform measured at sensor S_2 since they are far distant from the impact point and nearest to the edge of the plate. In the direct wave region, in order to remove the effect of the reflection wave, the band pass filter is used. After filtering, in the region of direct wave, the simulated waveforms are well corresponding with the measured waveforms. The spectrum of impact load $\hat{f}(\omega)$ used for the impact is shown in Fig. 5. In this paper, our purpose is to determine this force with waveforms measured by only three sensors and with the Green's function theoretically obtained by using the exact solution and the approximated SDPT. This is processed after determining the location of the impact load. For isotropic materials, the location of the impact load from the time difference from a pair of sensors can be shown to lie on a hyperbola with the two sensors as foci. For planar location, to uniquely locate the source, three sensors must be used. Tobias [6, 37], approached the problem as three intersecting circles, each centered at a sensor, with their radii determined by the time of propagation of the wave from the source to the respective sensor. By solving three resulting equations simultaneously he was able to find a closed form solution at a reference origin, and the angle, θ, from a reference axis. For three sensors, S_0, S_1 and S_2, located at (0,0), (x_1,y_1) and (x_2,y_2), respectively, these equations are

$$r = \frac{A_1}{2(x_1\cos\theta + y_1\sin\theta + \delta_1)} = \frac{A_{12}}{2(x_2\cos\theta + y_2\sin\theta + \delta_2)} \tag{14}$$

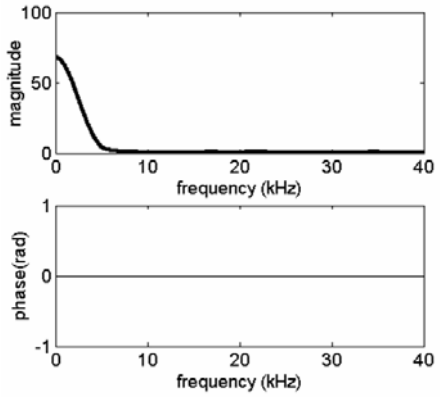

Fig. 5. Frequency spectrum of impact force measured throughout force transducer.

where

$A_1 = x_1^2 + y_1^2 - \delta_1^2$ and $A_2 = x_2^2 + y_2^2 - \delta_2^2$, $\delta_1 = t_1 c$ and $\delta_{21} = t_2 c$, c is the propagation velocity, and t_1 and t_2 are the time differences between sensor S_0-S_1 and S_0-S_2 respectively. For the angle θ,

$$\cos(\theta - \varphi) = K, \tag{15}$$

where

$$K = \left[\left(A_2\delta_1 - A_1\delta_2\right)/B\right] \tag{16}$$

$$B = \left[\left(A_1x_2 - A_2x_1\right)^2 + \left(A_1y_2 - A_2y_1\right)^2\right]^{1/2} \tag{17}$$

and

$$\tan\varphi = \left[\left(A_1y_2 - A_2y_1\right)/\left(A_1x_2 - A_2x_1\right)\right] \tag{18}$$

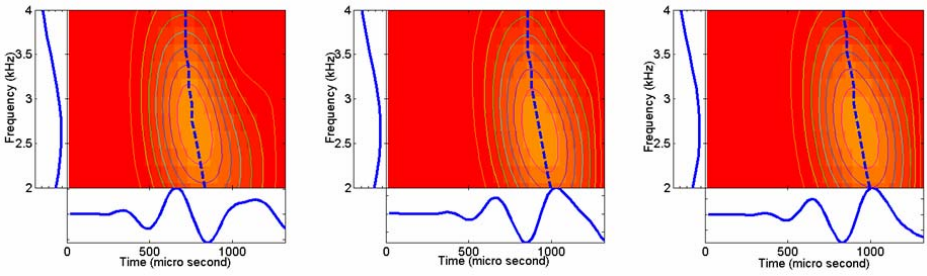

Fig. 6. CHOFT for the filtered measurement waveform (a) Sensor S_2 (b) Sensor S_0 (c) Sensor S_1.

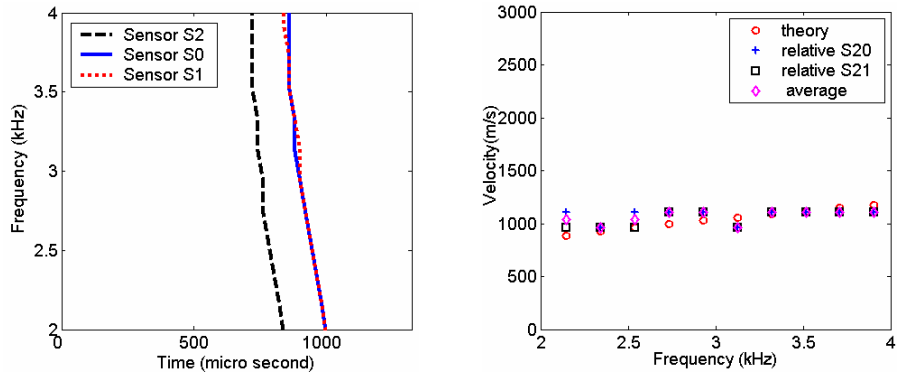

(a) (b)

Fig. 7. Arriving time difference for the waveform measured by the sensor S_0, S_1 and S_2 (a) Peak line obtained from image analysis using CHOFT (b) Group velocity for dispersive wave.

Thus, the quantities to be extracted from the waves are the time differences between the sensors and group velocity. Therefore, for the estimation of their radii, the propagation velocity also is required. For the dispersive wave, it was not easy to measure the group velocity using the traditional method [11]. After the time-frequency method is introduced, the measurement of group velocity becomes easy and the method becomes very familiar [6, 22]. According to previous research, the arriving time of Lamb modes is determined by a function of frequency from the corresponding peak in the time-frequency domain. The group velocity dispersion is the calculated by using the measured peak times as a function of frequency for the different modes, together with the known propagation distance. In order to estimate the arriving time and group velocity, the CHOFT for the filtered measurement waveforms as shown in Fig 4 is calculated and its image is plotted as shown in Fig. 6, respectively. The dotted line in the middle part is the peak line in CHOFT. Peak lines in Fig. 6 are selected and are plotted as shown in Fig. 7(a). Using these peak lines, the group velocity is calculated by dividing the known distance. The calculated group velocity is plotted as shown in Fig. 7(b). Relative S20 means the group velocity using relative time difference between sensor S_2 and S_0. Relative S21 means the group velocity using relative time difference between sensor S_2 and S_1. Average group velocity is the mean value of S20 and S21. The group velocities obtained by using different arriving times are very similar to the theoretical group velocity, which is calculated theoretically as shown in Fig. 8. With the group velocity and time difference, the location of impact load is estimated. Fig. 9 shows the estimated location of impact load using a group velocity of 2kHz as shown in Fig. 7(b). Fig. 10 shows the estimated location of sources using measured group velocity and theoretical group velocity. Fig. 10(a) shows the location of source, and Fig. 10(b) shows the distance error. According to these results, the estimation using the measured group velocity is better than that using theoretical group velocity. To identify the source location, the waveform of low frequency is used because the measured signal has reflection effect at high frequency and sampling time is 50kHz. For the identi-

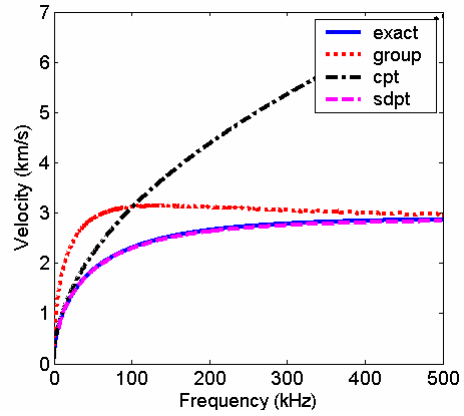

Fig. 8. Comparison of propagation wave velocity for a flexible wave in an aluminum plate.

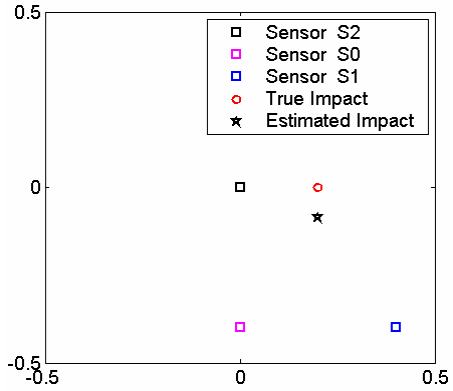

Fig. 9. Estimation of source location using measured group velocity at 2 kHz.

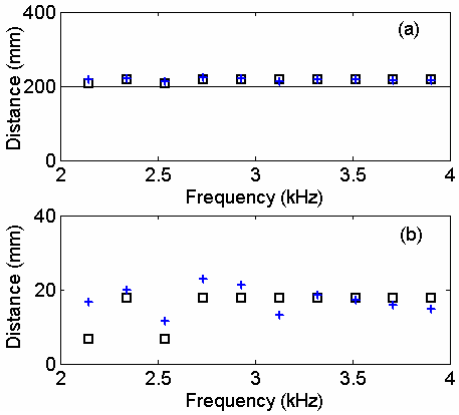

Fig. 10. Comparison between estimation of source location using the measured group velocity and estimation of source location using theoretical group velocity. (a) Distance from true source: (d) Distance error: (+) Using theoretical group velocity (□) Using measured group velocity.

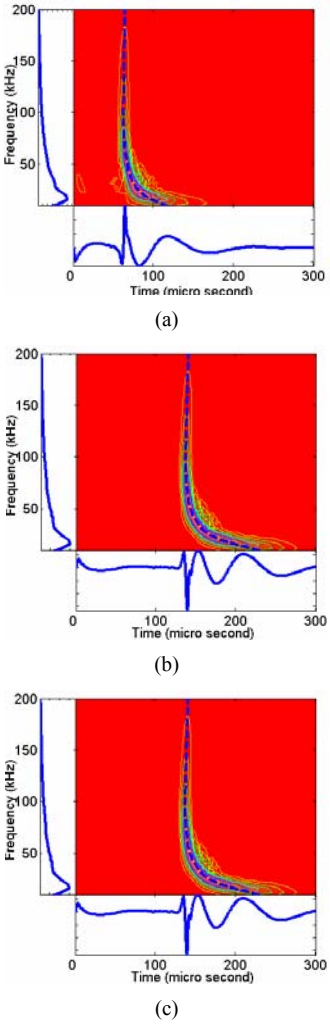

Fig. 11. CHOFT for the waveform simulated by the approximated SDPT (a) Position at sensor S_2 (b) Position at sensor S_0 (c) Position at sensor S_1.

fication of location source at high frequency, the simulated signal can be used. The impact load is a delta function $\delta(t)$. The spectrum of force is unity at the whole frequency. The band pass filter from 10kHz to 200kHz is used for this analysis. Fig. 11 shows the CHOFT for the simulated waveform using the approximate SPDT. In the image of CHOFT, the dispersion of only A0 mode is clear. Fig. 12(a) is the peak line obtained from image of three CHOFT as shown in Fig. 11. It gives the information on arriving time difference and group velocity. From 10kHz to 70kHz, the group velocity is overestimated compared to the theoretical group velocity. Using the group velocity at 50kHz, the source location is estimated and plotted as

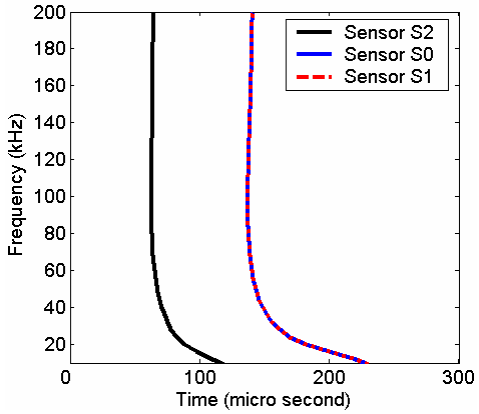

(a)

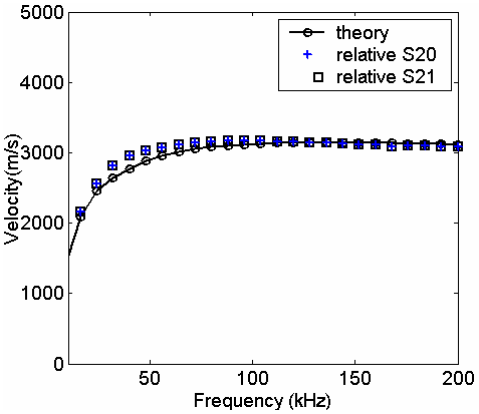

(b)

Fig. 12. Arriving time difference for the waveform simulated by the approximated SDPT (a) Peak line obtained from image analysis using CHOFT (b) Group velocity for dispersive wave.

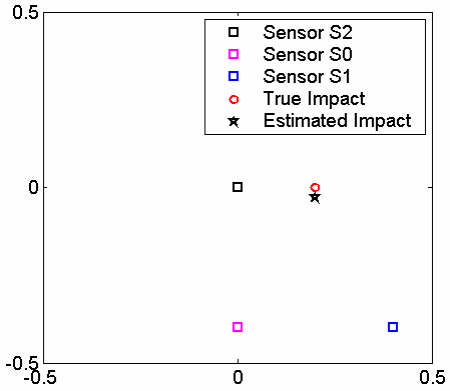

Fig. 13. Estimation of source location using group velocity at 2kHz for the simulated waveform obtained by the approximated SDPT.

shown in Fig. 13. Fig. 14 shows the estimated location of sources using measured group velocity and theoretical group velocity. Fig. 14(a) shows the location of source and Fig. 14(b) shows the distance error. The distance error is very small and the estimation of location is excellent. Fig. 15 shows the CHOFT for the simulated waveform using the approximate SPDT. Fig. 16(a) shows the peak lines obtained from image of three CHOFT as shown in Fig. 15. It gives the information arriving time difference and group velocity. From 10kHz to 70kHz, the group velocity is almost the same as the theoretical group velocity. Using the group velocity at 50kHz, the location of the source is estimated and plotted as shown in Fig. 17. It is much closer to the true position. Fig. 18 shows the estimated location of sources using measured group velocity and theoretical group velocity. Fig. 18(a) shows the location of source and Fig. 18(c) shows the distance error. The distance error estimated by using exact theory is much smaller than the distance error estimated by approximated SPDT. From 10 kHz to 70kHz because at high frequency, the group velocity waveform simulated by the approximated SPDT is overestimated. Fig. 19 shows this overestimation throughout the comparison of the waveform at high frequency obtained by using the approximate SPDT and that by using exact solution, whilst at low frequency this overestimation does not appear throughout comparison of the waveform obtained by using

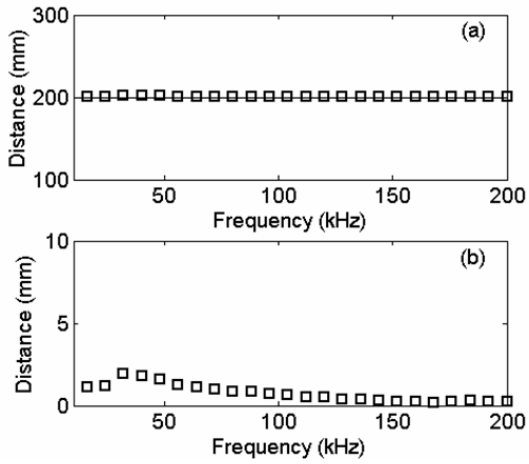

Fig. 14. Estimation of source location and distance error using the group velocity for the simulated waveform obtained by the approximated SDPT (a) Distance from true source (b) Distance error.

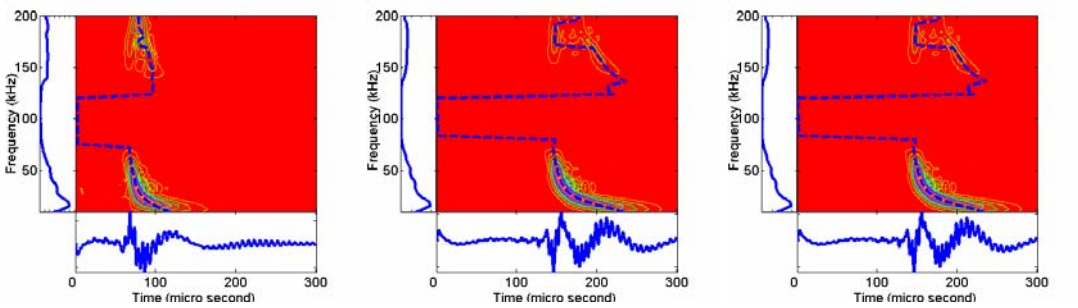

(a) (b) (c)

Fig. 15. CHOFT for the waveform simulated by the exact theory (a) Position at sensor S_2 (b) Position at sensor S_0 (c) Position at sensor S_1.

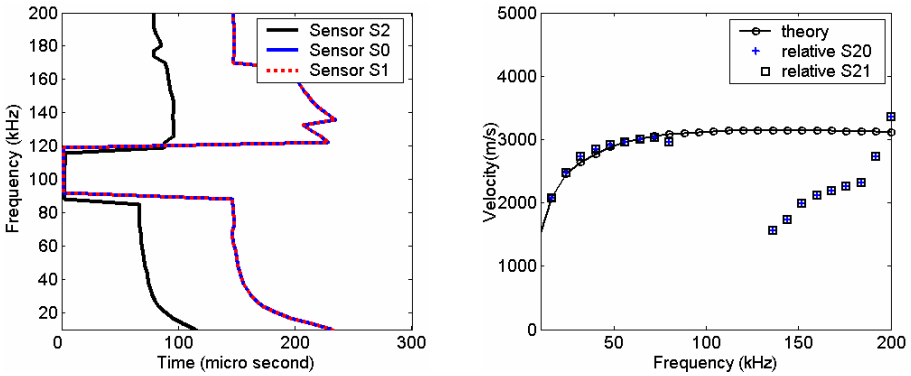

(a) (b)

Fig. 16. Arriving time difference for the waveform simulated by the exact theory (a) Peak line obtained from image analysis using CHOFT (b) Group velocity for dispersive wave.

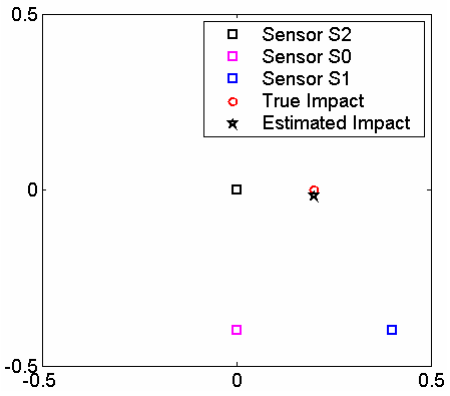

Fig. 17. Estimation of source location using group velocity at 50kHz for the simulated waveform obtained by the exact theory.

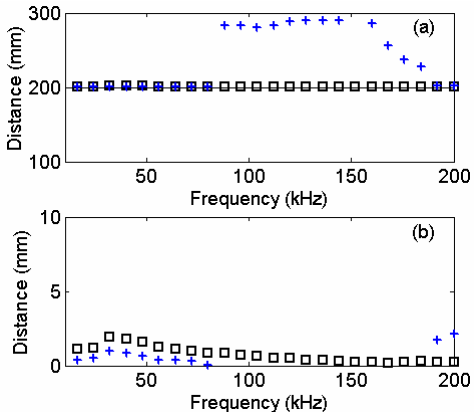

Fig. 18. Estimation of source location and distance error using the group velocity for the simulated waveform obtained by the exact theory. (a) Distance from true source (b) Distance error: (+) Using exact solution (□) Using approximated SDPT.

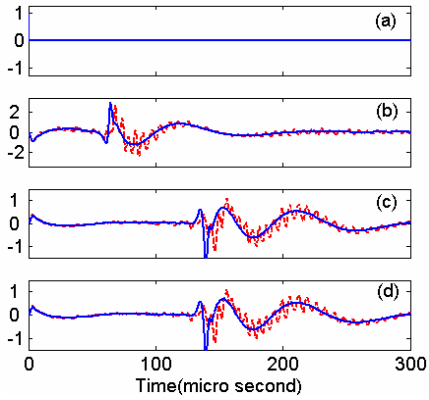

Fig. 19. The simulated waveforms by using the approximated SPDT at high frequency between 10kHz to 200kHz (a) Force $f(t) = \delta(t)$ (b) Waveform at Sensor S_2 (c) Waveform at Sensor S_0 (d) Waveform at Sensor S_1.

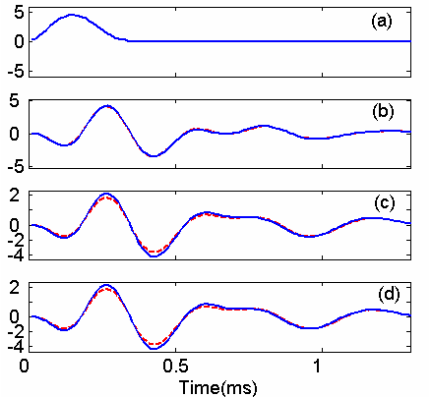

Fig. 20. The simulated waveforms by using the approximated SPDT at low frequency between 2kHz to 4kHz (a) Measured force (b) Waveform at Sensor S_2 (c) Waveform at Sensor S_0 (d) Waveform at Sensor S_1.

the approximate SPDT and that by using exact solution as shown in Fig. 20. At very high frequency over 70kHz, because the other lamb modes exist except A_0 mode, the method using exact solution is not a good estimator for the location of impact load because of the effect of the other lamb modes. However, it is a very good estimator for the location of impact load when the group velocity and arriving time difference at high frequency obtained by using the approximate SPDT are applied to the estimation of impact load.

5. Determination of impact load

As indicated earlier, the time dependence of the impact load can be recovered by deconvolving the waveforms measured at each sensor with the Green's functions. The theoretical Green's functions are the normal components of the displacement at the sensor locations due to a normal concentrated force of time dependence $\delta(t)$ at the impact location. They can be obtained from the exact formulation or the approximate SDPT using the procedure described in Ref. [26]. Since the accelerations are measured in the experiments, they are obtained from the displacements through careful double differentiations of the displacements. The time histories of these Green's functions using accelerations are plotted in Fig. 21. Since the measured accelerations include the waves reflected from the edges of the plate, while the calculated Green's functions are for a plate of infinite lateral dimensions, the time duration of the measured response used for the estimation the time history of impact load is selected to eliminate these reflections. In this study, 0.6ms is selected as the time duration because the propagation energy of the direct waveform is concentrated in that range as shown in Fig. 21. The reflected part in the measured is replaced by zero padding. The time history of the estimated impact load is compared with that of true impact in Fig. 22. The figures in the top row of Fig. 23 show the comparison between the measured impact load and the estimated impact load, while those in the bottom row show their Fourier transforms. According to these results, the impact load is very well estimated by using the impulse response at S_2, although there is some error due to the error in the estimated location. The estimations of the impact load using the impulse response at S_0 and S_1 also have some errors.

6. Conclusions

The location and time history of an impact load on a thick aluminum plate is identified through the use of the time-frequency method and deconvolution with the theoretical Green's function. An instrumented impact hammer is used as the application of the impact load on the plate surface and the waves generated by the load are recorded by three accelerometers located on the same surface. The location of the impact load is determined from the arrival time and group velocity of the waves by using the time-frequency analysis. The CHOTF is examined for simulated as well as measured waveform signals. It is found that the CHOTF is effective in detecting dispersive waves. The CHOFT is applied to the meas-

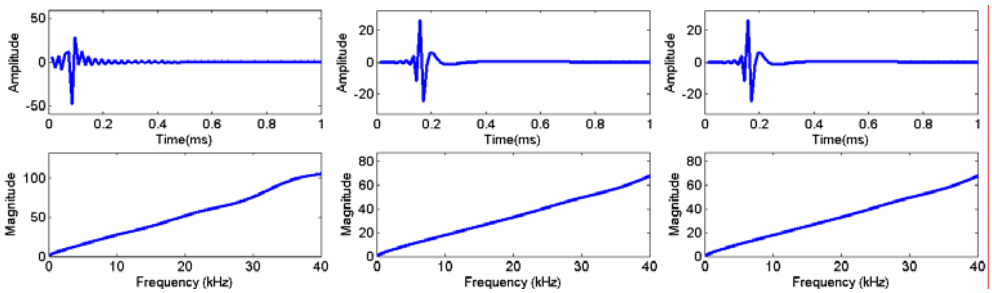

Fig. 21. Theoretical Green's functions $g(t)$ between the impact point and sensors S2 in the plate are obtained by using the approximated SDPT.

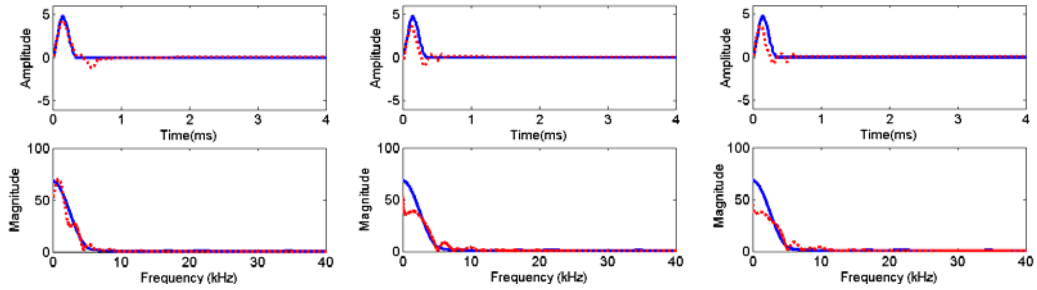

Fig. 22. Comparison between the measured true impact load and the estimated impact load and the comparison between the spectrum of measured impact load $\hat{f}(\omega)$ and that of the estimated impact load. (—)time history of true impact, (----) time history of estimated impact load (a) Sensor S_2 (b) Sensor S_0 (c) Sensor S_1.

ured and simulated waveform signals at three sensors due to the impact load. The location of the impact load is effectively estimated by using this arrival time and group velocity of the waves. The time history of the impact load is recovered by deconvolving the waveforms measured at three sensors with the calculated Green' functions. The estimated time history of the impact load compares well with that of the true impact if minor deviations in the estimated source location and the presence of reflected waves in the measured signal are discounted.

Acknowledgments

Authors thank Prof. A. K. Mal in Mechanical Engineering and Aerospace Engineering Department, University of California, Los Angeles for his permission about electrodynamics software.

Reference

[1] J. E. Michaels and Y. H. Pao, Determination of dynamic forces from wave motion measurements, *J. Appl. Mech*., 53 (1986) 61-68.

[2] L. Gaul and S. Hurlebaus, Determination of the impact force on a plate by piezoelectric film sensors, *Archiv. Appl. Mech.,* 69 (1999) 691-701.

[3] C. S. Yen and E. Wu, On the inverse problem of rectangular plates subjected to elastic impact, part I: method development and numerical verification, *J. Appl. Mech.,* 62 (1995) 692-697.

[4] M. Tracy and F. K. Chang, Identifying impacts in composite plates with piezoelectric strain sensors, part I: Theory, J. *Intelligent Material System and Structures,* 9 (1998) 920-928.

[5] S. Banerjee and A. K. Mal, Analysis of transient Lamb waves generated by dynamic surface source in thin composite plates, *J. Acoust. Soc. Am.,* 115 (2004) 1905–1911.

[6] S. M. Ziola and M. R. Gorman, Source location in thin plates using cross-correlation, *J. Acoust. Soc. Am.,* 90 (1991) 2551-2556.

[7] K. Kishimoto, H. Inoue, M. Hamada and T. Shibuya, Time frequency analysis of dispersive waves by means of wavelet transform, *J. Appl. Mech.,* 62 (1995) 841-846.

[8] L. Gaul and S. Hurlebaus, Identification of the impact location a plate using wavelets, *Mech. Sys. Sig-*

nal Process., 12 (1997) 783-795.

[9] M. R. Gorman, Plate wave acoustic emission, *J. Acoust. Soc. Am.,* 90 (1990) 358–364.

[10] W. H. Prosser and M. R. Gorman, Plate mode velocities in graphite/ epoxy plates, *J. Acoust. Soc. Am.,* 96 (1994) 902-907.

[11] W. H. Prosser, M. D. Seale, and B. T. Smith, Time-frequency analysis of the dispersion of Lamb modes, *J. Acoust. Soc. Am.,* 105 (1999) 2669-2676.

[12] A. K. Mal, C.-C. Yin and Y. Bar-Cohen, The influence of material dissipation and imperfect bonding on acoustic wave reflection from layered solids, *Rev. Prog. Quant. Nondestr. Eval.,* 7B (1988) 927-934.

[13] K. Balasubramaniam and J. L. Rose, Physically based dispersion curve feature analysis in the NDE of composites, *Res. Nondestruct. Eval.,* 3 (1991) 41-67.

[14] N. A. Schumacher, C. P. Burger and P. H. Gien, A laser-based investigation of higher-order modes in transient lamb waves, *J. Acoust. Soc. Am.,* 93 (1993) 2981-2984.

[15] D. Alleyne and P. Cawley, A two-dimensional Fourier transform method for the measurement of propagating multimode signals, *J. Acoust. Soc. Am.,* 89 (1991) 1159-1168.

[16] T. Önsay and A. G. Haddow, Wavelet transform analysis of transient wave propagation in dispersive medium, *J. Acoust. Soc. Am.,* 95 (1994) 1441-1449 .

[17] S. K. Lee, A Acoustic Decay Measurement Based on Time-Frequency Analysis Using Wavelet Transform, *J. Sound Vib.,* 252 (2002) 141-152.

[18] S. K. and S. U Lee, Reverberation time measurement for an acoustic room with low value of BT by utilizing wavelet transform, *J. Sound Vib.,* 275 (2004) 1101-1112.

[19] M. Niethammer, L. J. Jacobs, J. Qu and J. Jarzynski, Time-frequency representations of Lamb waves, *J. Acoust. Soc. Am.,* 109 (2001) 1841-1847.

[20] T. J. Wahl and J. S. Bolton, The application of the Wigner distribution to the identification of structure-borne noise components, *J. Sound Vib.,* 163 (1993) 101-122.

[21] R. Latif, E. H. Aassif, G. Maze, A. Moudden and B. Faiz, Determination of the group and phase velocities from time-frequency representation of Wigner-Ville, *NDT&E international,* 32 (1999) 415-422.

[22] S. K. Lee, Identification of wave propagation on the beam by using combined higher order time-frequency method, *Key Engineering Materials,* 270 (2004) 1466-1471.

[23] S. K. Lee and P. R. White, Fault diagnosis of rotating machinery using Wigner higher order moment spectra, *Mech. Sys. Signal Process,* 11 (1997) 637-650.

[24] S. K. Lee and P. R. White, Two-stage adaptive line enhancer and sliced Wigner trispectrum for the characterisation of faults from gearbox vibration data, ASME Trans. *J. Vib. Acoust.,* l21 (1999) 488-512.

[25] R. D. Mindlin, Influence of rotatory inertia and shear flexural motion of isotropic, elastic plate, *J. Appl. Mech.,* 18 (1951) 31-38.

[26] A. K. Mal, Elastic waves from localized sources in composite, International *Journal of Solids and Structures,* 39 (2002) 5481-5494.

[27] S. S. Lih and A. K. Mal, On the accuracy of approximate plate theories for wave field calculations in composite laminates, *Wave Motion,* 21 (1995) 17-24.

[28] R. Koenig, The Sound Spectrogram, *J. Acoust. Soc. Am.,* 18 (1946) 19-46.

[29] L. Cohen, Time-Frequency Analysis, Prentice hall, New Jersey, (1995).

[30] J. Ville, Theorie et Applications de la Notion de Signal Analytique, *Cables Transm.,* 2a (1948) 61-74.

[31] J. R Fonollosa and C. L. Nikias, Wigner-higher-order moment spectra definition, properties, computation and application to transient signal analysis, *IEEE Trans. Signal Process,* 41 (1993) 245-266.

[32] L. Stanković, A multitime definition of Wigner higher order distribution: L-Wigner distribution, *IEEE Signal Process. Letter,* 1 (1994) 106-225.

[33] L. Stanković, L-Class of Time- Frequency Distributions, *IEEE Signal Process. Letter,* 3 (1996) 22-25.

[34] S. K. Lee, A new method of smoothing non-oscillation cross-terms in sliced Wigner fourth order moment spectra, *Mech. Sys. Signal Process,* 15 (2001) 1023-1029.

[35] L. Stanković, Auto-term representation by the reduced interference distribution: a procedure for kernel design, *IEEE Trans. Signal Process,* 44 (1996) 1557-1563.

[36] S. K. Lee, Adaptive Signal Processing and Higher Order Time Frequency Analysis for Acoustic and Vibration Signatures in Condition Monitoring, Ph.D. Thesis, University of Southampton, (1998).

[37] A. Tobis, Acoustic Emission Source Location in two dimensions by an array of three sensors, *Non-*

Destructive Testing, 9 (1976) 9-12.

[38] S. K. Lee, Identification of Impact Force in Thick Plates Based on the Elastodynamics and Time-Frequency Method (Part I: Theoretical Approach for Identification the Impact Force Based on Elastodynamics), The Journal of Mechanical Science and Technology, Submitted paper (2008).